 doi:10.20944/preprints202205.0177.v1

Article

Evaluation of Axial Compression Slenderness Limits of High and Very-High Strength Steel Circular Hollow Sections

Fattouh M. F. Shaker[1], Kyrolos Zarzor [2], Sameh Gaawan [1], Ahmed Deifalla [3*] and Mohamed M. A. Salem[1]

[1] Staff member at civil Eng. Department, Faculty of Eng. Mataria, Helwan University, Egypt; fatouhm@hotmail.com
[2] Demonstrator, at Faculty of Eng. Mataria, Helwan University, kyroloszarzor1@gmail.com.
[3] Structural engineering and construction management department, Future University in Egypt; ahmed.deifalla@fue.edu.eg
* Correspondence: ahmed.deifalla@fue.edu.eg; diffalaf@mcmaster.ca.

Abstract: Despite significant advances in metallurgy and the potential to create high and very high-strength steel, all international specifications for steel design provided little information about the limits of slenderness for high-strength steel sections (*HSSs*) and didn't give anything about the design of very high-strength steel sections (*VHSSs*). The American structural steel design specification covers circular hollow sections (CHS) of steel grades up to S690, while it isn't in *ANSI/AISC 360-16* and *ASTM A514/A514M*. Euro code *EN 1993-1-1* can be applicable only to steel grades up to S460. *EN 1993-1-3* and *EN 1993-1-12* contain supplementary rules for cold-formed members and *HSS* (S460- S700), respectively. Though ductility requirements for (*HSS)* are specifically established in *EN 1993-1-12*, it is largely a continuation of the normal-strength-steel design procedures standardized in *EN 1993-1-1*, where (*HSSs*) are largely treated as normal-strength steels in these rules, and the same design approaches are used. The behavior of high and very high-strength steel circular hollow sections under axial compression load is studied in this research. A total of 16 nonlinear finite-element (FE) models were generated to replicate stub column tests that were experimentally tested by others in previous research. Hence, a parametric study is conducted using forty FE models developed to investigate the local buckling behavior under various slenderness ratios comprehensively. The developed models cover slenderness ratios ranging from 20 to 1226 and steel grades S460 and S1100 with yield stress equal 460Mpa and 1152Mpa, respectively. The FE results were combined with 105 previously collected experimental results to assess the applicability of existing codified design methodologies in the Euro code and the North American codes of cold-formed CHS. Based on the results of this study, new cross-sectional slenderness limits and new design equations for more efficient simple designs were presented for high and very-high strength steel circular hollow sections and Compared with the results of experimental tests and FE models.

Keywords: cross-section resistance; slenderness limit; high strength steel; tubular sections; very-high strength steel; cold-formed; thin-walled circular hollow sections; finite element analysis; ANSYS

1. Introduction

Since the early 1800s, circular hollow sections (*CHS*) have been used in the construction field as columns, beams, tension members, and truss elements [1]. They have gained the designers' preferences due to their appealing aesthetics and advantages over open sections. In addition, the *CHS* profiles possess superior torsional resistance, bi-axial bending resistance, reduced drag of wind loads, the ability to be filled with concrete to form composite sections, and lower maintenance requirements due to smaller external areas exposed corrosive environments [1]. *CHS* is primarily thin-walled structural elements, and thus local buckling, whether before or after material yielding, becomes the primary factor in their design. Cross-section classification is used in current design codes, which

 doi:10.20944/preprints202205.0177.v1

divides the circular hollow sections (*CHS*) into distinct categories based on their sensitivity to local buckling. The European Committee for Standardization, *EN 1993-1-1* [2], and the British Standard Institution, *BS 5950-1* [3] for structural steelwork, EN 1993-1-4 [4] for stainless steel, and *EN 1999-1-1* [5] for aluminum, consider four cross-section classes. Class 1 cross-sections can reach and sustain their full plastic moment capacity [M_{pl}] while maintaining adequate rotation capacity for plastic design. Class 2 cross-sections can reach their full plastic moment capacity with limited rotational capacity. However, the *AISC 360-16* [6] and *AS 4100* [7] steel codes have no equivalent European class 2 cross-section classification. Due to local buckling, Class 3 cross-sections cannot attain their plastic moment capacity, and their bending capacity is restricted to the elastic moment capacity [M_{el}]. In Class 4 cross-sections, local buckling occurs before reaching the elastic moment capacity, and thus class 4 sections are commonly referred to as slender sections. Moment-rotation capacity and idealized bending stress distributions associated with the four classes are illustrated in Fig. (1), respectively. The class 3 limit in terms of axial resistance distinguishes non-slender cross-sections that can attain yield load without any local buckling (i.e., classes 1–3) from those that fail before reaching their yield load due to local buckling (i.e., class 4).

To date, *HSS-CHS* columns have been studied to explore more effective design methods [9,10]. Martin D. O'Shea [11] studied the local buckling of slender circular steel sections experimentally by testing 39 *CHS* stub columns with yield stresses ranging from 210 to 363 MPa. Chung et al. [12] investigated the ultimate strengths of high-strength thin-walled square *CFST* slender beam-columns under axial and uniaxial loads with yield stresses of 445 MPa. Lan hui Guo et al. [13] studied the behavior of thin-walled circular hollow section stub columns subjected to axial compression with yield stresses of 190 MPa. Wang Hui et al. [14] studied the stability capacity of High-strength Circular Steel Tubes Under Axial compression with yield stresses of 690 MPa. The sectional capacity of very high-strength steel CHSs was examined by Xiao-Ling Zhao [15]. The yield stresses of these specimens were as high as 1,350 MPa. Jiao and Zhao [16] conducted experimental studies on 8 *CHS* stub columns to evaluate the slenderness limit of very high-strength *CHSs*. Recently, Jia-Lin Ma et al. [17] investigated the stub column behavior of *HSS-CHSs*. Twenty-five specimens were tested with yield stresses varying from 700 to 1100 MPa.

Despite the rapid development in metallurgy and the ability to obtain types of steel with high and very high strength, all international specifications for steel design gave little information about the limits of slenderness and design of high-strength steel sections and didn't give anything about very-high strength steel sections specially *CHS*. Therefore, the main objects of this study are to study the behavior of high and very-high strength (*CHS*), evaluate the current slenderness limit in different codes, and assess the current formulae of EC3 and AISC for the design of high strength steel circular hollow sections (*HSS-CHS*) and suggesting design equations that can be used to accurately calculate the limit of slenderness for (*HSS-CHS*) and (*VHSS-CHS*). To achieve these objectives, forty finite element models are carried out using ANSYS to verify the accuracy of the results of the experimental tests carried out by other researchers, as detailed in the literature review for 105 CHS stub columns covering a wide range of cross-section slenderness ratios.

2. Background on current design methods for carbon steel cross-sections and slenderness limits

The concept of cross-section classification is the currently adopted approach for identifying local buckling in metallic sections and is used to determine the appropriate structural design strength. *EN 1993-1-3* [18] uses the *EN 1993-1-1* technique for carbon steel hot rolled cross-section classification, with the yield stress f_y taken as 0.2% of the proof stress and a sequence of width-to-thickness ratios (b/t) in terms of material properties. In addition, the type of edge support (internal or external) and the type of applied stress are specified. The overall cross-section classification is assumed to depend on the thinnest constituent element, ignoring the advantages of element interaction. Slenderness limits are often

Preprints (www.preprints.org) | NOT PEER-REVIEWED | Posted: 13 May 2022 doi:10.20944/preprints202205.0177.v1

determined based on experimental results at the cross-section level. Analysis of results by Gardner [19], based on a more comprehensive experimental database, has shown that the current classification limits are too conservative and may, in many cases, be enhanced as conducted by O'Shea, Gardner, and Zhao [11, 19, 20]. In addition to the problem of classification slenderness limits, there is another problem related to the limitations of applying current code design rules to very-high strength steel (*VHS*). Because the current Euro code *EN-1993-1-12* [21] includes supplementary rules that allow the use of steel grades up to S700. *EN-1993-1-3* indicated cold-formed circular structural hollow sections supplied to *EN10219-1* [22], which should be referred to as *EN-1993-1-1* in cold-formed steel standards. American Specification *AISC360-16* allows high-strength steel with yield strength up to 690 MPa for plates [23] and 485 MPa for hollow structural sections [24]. North American Specification *AISI-S100-12* [25] allows high strength steel with yield strength up to 450 MPa, which complies with the high strength steel according to the ASTM standards. Therefore, the design of *VHS* tubes (with yield stress over 1000 MPa) cannot be designed directly by using these standards' rules.

The nominal strength of Class 1–3 cross-sections in compression is specified in the *EN 1993-1-1* as determined by Eq (1). *EN 1993-1-6* employs shell buckling theory to determine the axial compressive strength of shell elements, which is suitable for the cases of *CHS* members class 4. Accordingly, the corresponding nominal resistance of shells in compression can be obtained from Eq (2). The nominal compressive strength of cross-sections subjected to yielding or local buckling in *ANSI/AISC 360-16* and *AISI-S100-12* can be calculated from equations (3) and (4), respectively.

$$N_{EC3\text{-}1\text{-}1} = f_y * A \qquad \text{for } \frac{D}{t} \le (90*\varepsilon^2) \quad (EN\ 1993\text{-}1\text{-}1, [2]) \tag{1}$$

$$N_{EC3\text{-}1\text{-}6} = \chi * f_y * A \qquad \text{for } \frac{D}{t} \le (90*\varepsilon^2) \quad (EN\ 1993\text{-}1\text{-}6, [4]) \tag{2}$$

$$\text{Where} \quad \varepsilon = \left(\frac{235}{f_y} * \frac{E}{210}\right)^{0.5}$$

$$\lambda s = \left(\frac{D}{t} * \frac{f_y}{235}\right)$$

$$N_{AISC} = 0.658^{Q*f_y/f_e} * Q_f \qquad (ANSI/AISC\ 360\text{-}16, [4]) \tag{3}$$

$$N_{AISI} = f_n * A_e \qquad (AISI\text{-}\ S100\text{-}12, [4]) \tag{4}$$

Where: A: is the gross cross-sectional area, A_e is the effective cross-sectional area determined by the effective width method, E (Gpa) is the modulus of elasticity for steel, f_y (Mpa) is the steel yield stress, λ_s is the plate element slenderness, χ is the buckling reduction factor determined by the relative slenderness of the shell, Q is the reduction factor related to the effective cross-sectional area where it equals 1.0 for cross-sections without slender elements, f_e is the elastic buckling stress specified in Section *E3* of *ANSI/AISC 360-16*, and f_n is the global column stress determined following Section *E2* of *AISI-S100.*

When the previous Euro code and American Specification equations were used for High-strength steel (*S460*) and Very-high steel (*S1100*), the slenderness limit can be calculated as follows:

$$\frac{D}{t} \le (90*\varepsilon^2) = 90 * \left(\frac{235}{f_y} * \frac{E}{210}\right)$$

$$\frac{D}{t} \le 90 * \left(\frac{235}{460} * \frac{210}{210}\right) = 46 \qquad \text{for High-strength steel } (S460)$$

$$\text{And also } \frac{D}{t} \le 90 * \left(\frac{235}{1152} * \frac{207}{210}\right) = 18 \qquad \text{for Very-high-strength steel } (S1100)$$

Therefore, one of the main objectives of this study is to check the accuracy of using the previous Euro code and American Specification equations to determine the slenderness limits for (*S460*) and (*S1100*) by using finite element analysis.

3. Finite element simulation

Geometrically and materially nonlinear analyses with imperfection (GMNIA) [4] were performed by using ANSYS [27]. The F.E. models have been developed to best fit the properties of CHS sections under various loading scenarios. To determine the ultimate

Preprints (www.preprints.org) | NOT PEER-REVIEWED | Posted: 13 May 2022 doi:10.20944/preprints202205.0177.v1

resistance of a section numerically, shell element 181 was adopted as an element type. Models which are exposed to bending moment were first used to witness local buckling of the cross-section and due to the high torsional capacity of circular hollow sections; in such cases, the length of the specimens was chosen equal to twelve times the outer diameter of CHS in order to calculate the accurate rotation capacity through pure moment zone.

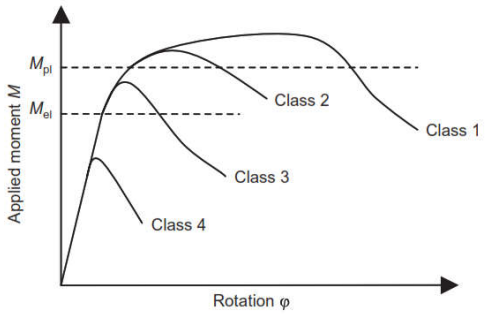

Figure 1. Moment–rotation response of four behavioral classes of cross-section [8].

3.1. Material properties

A true modified bilinear stress-strain curve was adopted, in which the initial linear region represents young's modulus E which is assumed to equal 210 and 207 Gpa for High-strength steel (S460) and Very High-strength steel (S1100) respectively as mentioned in previous experimental researches. The initial line ends up to a stress point defined as (f_y, ε_y), where f_y is taken as the material 0.2% proof stress and ε_y is the corresponding elastic strain $\varepsilon_y = E/f_y$. After that, it assumed that the material followed the linear hardening with a reduced hardening modulus E_r equal to $0.01E$. The used steel with specified yield stress f_y and ultimate strength f_u of *460 MPa* and *550 MPa*, respectively for HSS-S460 and equal 1152 Mpa, 1317 Mpa respectively for VHSS-S1100 [26, 29] as shown in Figure 2. Poisson's ratio is taken to equal 0.3.

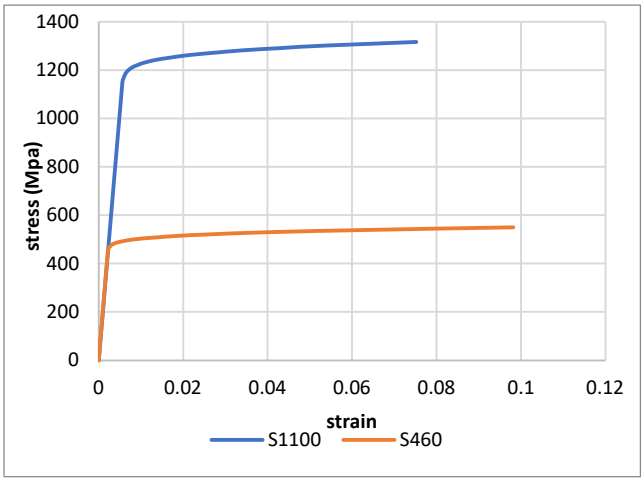

Figure 2. Stress-strain curve of modeled material.

3.2. Mesh refinement

Different types of mesh densities were tested under compression for CHS stub columns with length equal 3 times the diameter, where the selected meshing types ranged from fine (Type I meshing) to coarse (Type IV meshing), in order to examine the influence of the mesh refinement on cross section' resistance. The purpose of this study is to adopt the most appropriate mesh density, able to provide an accurate numerical prediction of the section's behavior at reasonable computation costs. Therefore, a series of F.E. models'

Preprints (www.preprints.org) | NOT PEER-REVIEWED | Posted: 13 May 2022 doi:10.20944/preprints202205.0177.v1

calculations were performed on circular hollow sections by considering the parameters listed in Table 1

Table 1. Parametric study for S460, to evaluate the best mesh size.

Cross-section	Type	Mesh size
CHS_508x2	I	(D/40)
5	II	(D/20)
10	III	(D/10)
16	IV	(D/5)

The obtained results of this comparison are shown in Figure 3 for different *CHS* sections. One directly observes that the coarse meshes (Type III and Type IV) do not lead to acceptable results, being by as much as 8% and 13% respectively lower than those of Type I mesh in the worst cases; therefore, these meshes have not been considered. Further, reasonable results and negligible differences are observed for denser meshes (Type I and Type II) for all sections. Accordingly, mesh Type II was selected as it leads to satisfactory results with minimal computational effort.

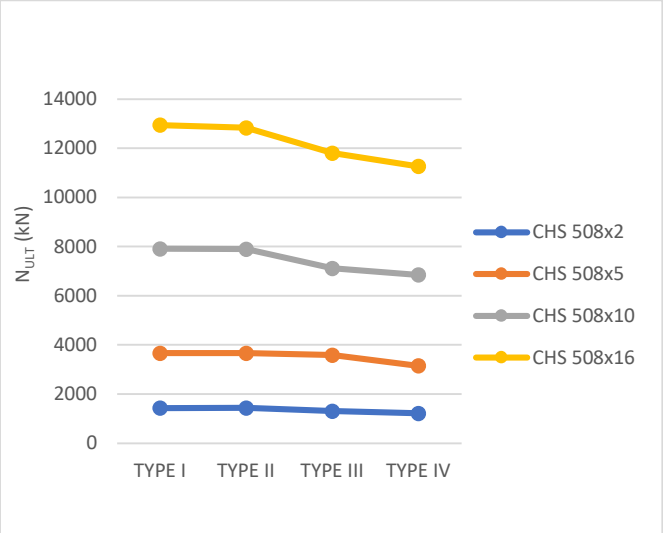

Figure 3. Mesh density study -results of CHS sections.

3.3. Loading and support conditions

The support conditions and the introduction of applied loads received particular attention. Following ideal simply-supported support conditions, one end of the cross-section can only exhibit a maximum of three degrees of freedom: axial global displacement, rotation about the strong and weak axis, the other end only exhibits a maximum of two degrees of freedom: rotation about the strong axis and rotation about the weak axis and only one point at the center was restrained against axial global displacement. External loading was applied through one concentrated force on a plate with a thickness 80 mm at the top for pure compression loading. Figure 4 shows the used finite element model.

Preprints (www.preprints.org) | NOT PEER-REVIEWED | Posted: 13 May 2022 doi:10.20944/preprints202205.0177.v1

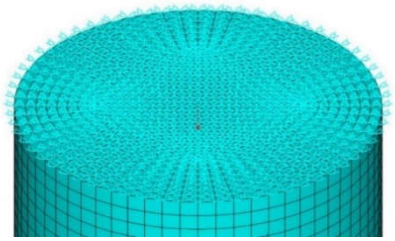

Figure 4. The used finite element model in a numerical study by authors.

3.4. Geometrical imperfections

In order to examine the influence of local initial imperfection on the member resistance, different shapes of initial local geometric imperfections were examined. Local imperfections shapes were introduced through an appropriate modification of node coordinates of the considered section through buckling analysis of deferent modes of shapes. Two-mode shapes were examined to select the most appropriate mode based on the ultimate resistance and the expected failure modes in comparison with experimental tests as shown in Figure 5. Case studies as detailed below show that chequerboard-mode can predict with reasonable accuracy the structural behavior of the sections and give appropriate failure mode in comparison with experimental mode shapes. Therefore, a series of F.E. models' calculations were performed on circular hollow sections by considering the length of the specimen to be three times its diameter concluded from previous research to cancel the effect of global buckling. The considered steel grade is S460, and the loading is axial compression The considered models are summarized in Table 2.

Table 2. parametric study for evaluating imperfection shape.

Cross-section	Mesh size
CHS_150x2	type I & type II
CHS_200x2	type I & type II
CHS_250x2	type I & type II
CHS_300x2	type I & type II
CHS_400x2	type I & type II

where type I is axisymmetric mode and type II is chequerboard mode. For each type of shape defined, a value of the amplitude $\Delta\omega$ in (Equation 5) was adopted, which depends on the fabrication quality parameter (Q) as clarified in Table 3. Q of 40 was chosen based on previous research [30], which concluded that most of the measured geometric imperfections of cold-formed CHS do not exceed the value that comes from Q=40.

$$\Delta\omega = \frac{1}{Q} * \sqrt{\frac{r}{t}} * t \tag{5}$$

Table 3. Values of fabrication quality parameter.

Fabrication quality class	Description	Q
Class A	*Excellent*	*40*
Class B	*high*	*25*
Class C	*normal*	*16*

Based on the previously-mentioned conclusions, the adopted local imperfection is type 2 and that's consistent with the procedure and assumptions adopted by X.Meng [31] that represents the most reasonable and realistic mode of imperfections as shown in Figure (6).

Preprints (www.preprints.org) | NOT PEER-REVIEWED | Posted: 13 May 2022 doi:10.20944/preprints202205.0177.v1

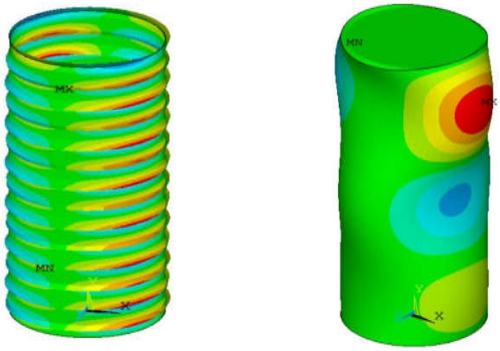

(a) Type 1 (b) Type 2

Figure 5. Imperfection shapes.

Figure 6. Magnified view of local imperfections.

3.5. Residual stresses

In cold-formed elements, residual stresses come from coiling and uncoiling, rolling, and welding. However, the dominant bending residual stresses for cold-formed sections are inherently incorporated into the stress-strain relationships obtained from the tensile coupon tests, therefore, the explicit inclusion of residual stresses into the FE models was deemed unnecessary which agrees with what Gardner conducted [32].

3.6. Validation

In order to verify the reliability of the proposed finite element model, the results obtained from the models using ANSYS software are compared with the results of experimental tests that were carried out by Lanhui Guo [33] as shown in Table 4. A finite element model using ANSYS software was conducted to resemble the failure mode and load-carrying capacity of circular hollow section *CHS*, which are conducted through an experimental study by Lanhui. The analytical models have shown a high degree of agreement with the experimental results in both load-carrying capacity and failure modes of the specimens. The Comparison between the failure modes obtained from the experimental tests by Lanhui Guo and the ANSYS models of this research is presented in Figure (7). In addition, the load-deflection curves obtained from the experimental tests and the ANSYS models are presented in Figure 8. From these figures, it is clear that the failure loads resulting from experimental tests are in good agreement with that resulting from the ANSYS models of this study.

Preprints (www.preprints.org) | NOT PEER-REVIEWED | Posted: 13 May 2022 doi:10.20944/preprints202205.0177.v1

Table 4. Geometric parameters of specimens tested by (Lanhui Guo and shilong) [33].

	D (mm)	t (mm)	L (mm)	D/t	L/D	Number of repeats
DT75	150	2	450	75	3	3
DT100	150	2	600	100	3	3
DT125	200	2	750	125	3	3
DT150	200	2	900	150	3	3
DT200	250	2	1200	200	3	2
DT300	250	2	1800	300	3	2

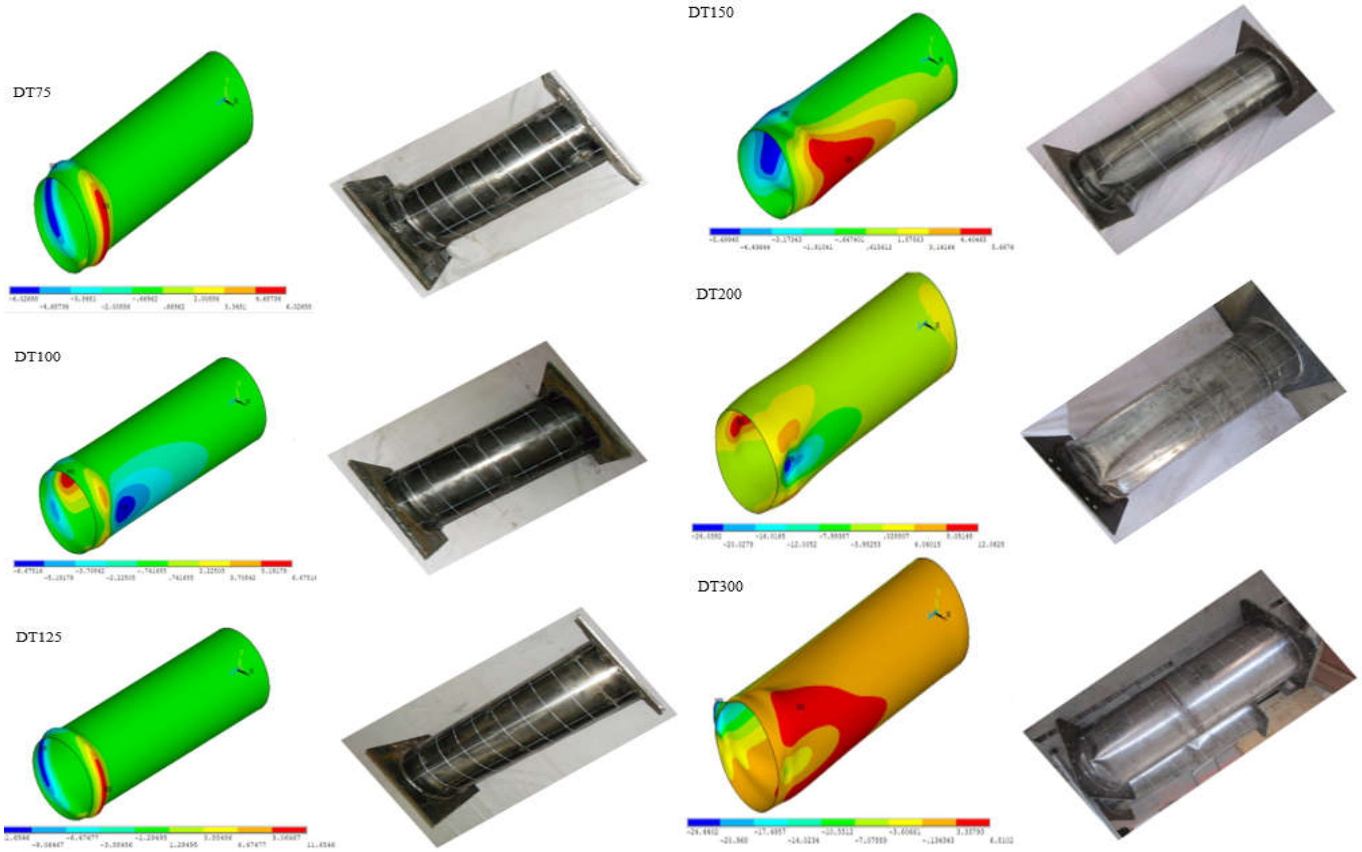

Figure 7. Comparison between failure phenomena resulted from FEA by authors and experimentally by Lanhui [33] for specimens with D/t= 75 to 300.

Preprints (www.preprints.org) | NOT PEER-REVIEWED | Posted: 13 May 2022 doi:10.20944/preprints202205.0177.v1

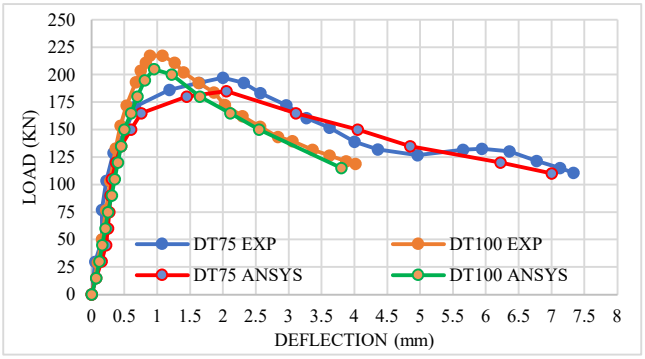

(a) specimens of D/t 75 and 100

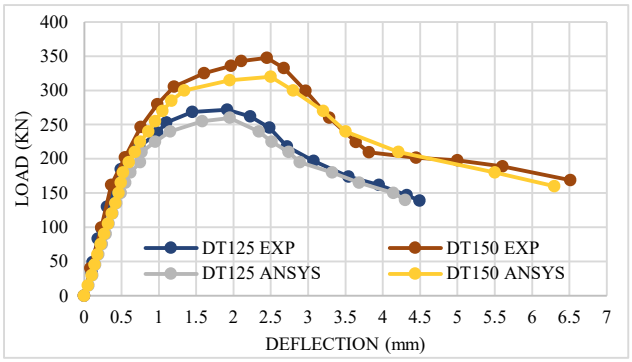

(b) specimens of D/t 125 and 150

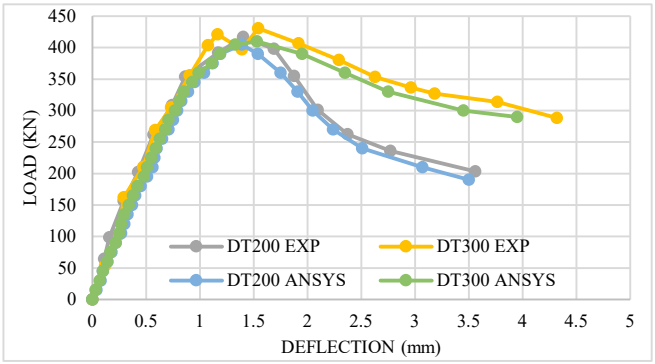

(c) specimens of D/t 200 and

Figure 8. Comparison between (P-Δ) resulted from FE by authors and experimental by Lanhui [33] for specimens with D/t= 75 to 300.

4. Parametric study

A number of 40 finite element models were modeled to study the behavior of (*CHS*) under axial compression load, Table 5. The parametric study is based on the determination of the Maximum axial compression load-carrying capacity of High and very-high strength steel slender and non-slender circular hollow sections for evaluating the design methods in the current codes of practice such as AISC 360-16 and EC3. In addition to attempting to specify a slenderness limit at which local buckling occurs. The results were presented and discussed to assess the effect of each parameter. Two parameters were taken into account and they were studied in order to determine the effect of each one separately. Therefore, 40 models with a twenty value of diameter to thickness (D/t) ratio ranging from 10 to 250 and two values of yield stresses of 460 Mpa and 1100 Mpa are considered in this study. The length to diameter ratio is assumed to equal 3 for all studied stub columns to rule out the effect of global buckling as concluded in much previous research such as Lanhui [33]. The geometric imperfection was taken into account based on EC3 code with fabrication quality parameters equal to 40 for all models.

Each model from the studied models is named to give information about its group and dimensions, for example, LC1-102-10-460. Where the first letter (LC1) refers to the name of the group, the first number (102) refers to the diameter (D) value in mm, the second number (10) refers to the thickness (t) value in mm, and the last number (460) refers to the yield stress value in Mpa.

Preprints (www.preprints.org) | NOT PEER-REVIEWED | Posted: 13 May 2022 doi:10.20944/preprints202205.0177.v1

Table 5. Dimensions and properties of the studied *CHS* high and very high strength steel stub columns.

No	Symbol	D (mm)	t (mm)	H (mm)	D/t	G.I$_{EC3}$ (mm)	Fy (MPa)	Fu (MPa)	Es (GPa)	$\frac{D}{t} * \frac{f_y}{235}$
1	LC1-102-10-460	101.6	10.0	304.8	10	0.56	460	550	210	19.9
2	LC1-219-10-460	219.1	10.0	657.3	22	0.83	460	550	210	42.9
3	LC1-324-10-460	323.9	10.0	971.7	32	1.01	460	550	210	63.4
4	LC1-406-10-460	406.4	10.0	1219.2	41	1.13	460	550	210	79.6
5	LC1-508-10-460	508	10.0	1524	51	1.26	460	550	210	99.4
6	LC1-102-1.7-460	101.6	1.70	304.8	60	0.23	460	550	210	117.0
7	LC1-219-3-460	219.1	3.00	657.3	73	0.45	460	550	210	143.0
8	LC1-324-4-460	323.9	4.00	971.7	81	0.64	460	550	210	158.5
9	LC1-406-4.5-460	406.4	4.50	1219.2	90	0.76	460	550	210	176.8
10	LC1-508-5-460	508	5.00	1524	102	0.89	460	550	210	198.9
11	LC1-220-2-460	220	2.00	660	110	0.37	460	550	210	215.3
12	LC1-240-2-460	240	2.00	720	120	0.39	460	550	210	234.9
13	LC1-260-2-460	260	2.00	780	130	0.40	460	550	210	254.5
14	LC1-280-2-460	280	2.00	840	140	0.42	460	550	210	274.0
15	LC1-300-2-460	300	2.00	900	150	0.43	460	550	210	293.6
16	LC1-320-2-460	320	2.00	960	160	0.45	460	550	210	313.2
17	LC1-360-2-460	360	2.00	1080	180	0.47	460	550	210	352.3
18	LC1-400-2-460	400	2.00	1200	200	0.50	460	550	210	391.5
19	LC1-450-2-460	450	2.00	1350	225	0.53	460	550	210	440.4
20	LC1-500-2-460	500	2.00	1500	250	0.56	460	550	210	489.4
21	LC1-102-10-1100	101.6	10.0	304.8	10	0.56	1152	1317	207	49.8
22	LC1-219-10-1100	219.1	10.0	657.3	22	0.83	1152	1317	207	107.4
23	LC1-324-10-1100	323.9	10.0	971.7	32	1.01	1152	1317	207	158.8
24	LC1-406-10-1100	406.4	10.0	1219.2	41	1.13	1152	1317	207	199.2
25	LC1-508-10-1100	508	10.0	1524	51	1.26	1152	1317	207	249.0
26	LC1-102-1.7-1100	101.6	1.70	304.8	60	0.23	1152	1317	207	293.0
27	LC1-219-3-1100	219.1	3.00	657.3	73	0.45	1152	1317	207	358.0
28	LC1-324-4-1100	323.9	4.00	971.7	81	0.64	1152	1317	207	396.9
29	LC1-406-4.5-1100	406.4	4.50	1219.2	90	0.76	1152	1317	207	442.7
30	LC1-508-5-1100	508	5.00	1524	102	0.89	1152	1317	207	498.1
31	LC1-220-2-1100	220	2.00	660	110	0.37	1152	1317	207	539.2
32	LC1-240-2-1100	240	2.00	720	120	0.39	1152	1317	207	588.3
33	LC1-260-2-1100	260	2.00	780	130	0.40	1152	1317	207	637.3
34	LC1-280-2-1100	280	2.00	840	140	0.42	1152	1317	207	686.3
35	LC1-300-2-1100	300	2.00	900	150	0.43	1152	1317	207	735.3
36	LC1-320-2-1100	320	2.00	960	160	0.45	1152	1317	207	784.3
37	LC1-360-2-1100	360	2.00	1080	180	0.47	1152	1317	207	882.4
38	LC1-400-2-1100	400	2.00	1200	200	0.50	1152	1317	207	980.4
39	LC1-450-2-1100	450	2.00	1350	225	0.53	1152	1317	207	1103.0
40	LC1-500-2-1100	500	2.00	1500	250	0.56	11520	1317	207	1225.5

4.1. Finite element results and discussion

Figures 9 and 10 show stress distributions through the tube length and failure mode of different specimens with D/t ratio ranging between 10 to 250 for high-strength steel (S460) and very high-strength steel (S1100) respectively. In general, it is observed that the position of failure for the most of specimens is located approximately at D/4 away from the

Preprints (www.preprints.org) | NOT PEER-REVIEWED | Posted: 13 May 2022 doi:10.20944/preprints202205.0177.v1

two ends. But for specimens that have slender sections with D/t > 200, it failed through overall its length.

It is found that the outward deformation was like an elephant's foot buckle, i.e., one notable outwards circumferential buckle occurred at the two ends of the tube. This shape of buckling developed into a plastic mechanism the smooth outward deformation was the typical failure mode of tubes with D/t ≤ 100 for high-strength steel (S460) and D/t ≤ 30 for very high-strength steel (S1100) respectively as shown in Figures 9 and 10. This failure is classified as a yield failure. The reason for this shape of deformation is that at this range of D/t, the specimens are in the hardening stage when they reach their peak load.

Figures 11 and 12 show the relation between stress–vertical strain curves of different specimens with D/t ratios ranging between 10 to 250 for high-strength steel (S460) and very high-strength steel (S1100) respectively. It is shown that the value of maximum stresses can exceed the yield value and up to reach the value of its ultimate stress for specimens tubes with D/t ≤ 100 for high-strength steel (S460) and D/t ≤ 30 for very high-strength steel (S1100) respectively. Therefore, according to the results of this numerical study, it is concluded that specimens with D/t up to equal 100 or 30 for high-strength steel (S460) or very high-strength steel (S1100) respectively behave as non-slender sections. This is completely different from what is inferred from slenderness limits according to Euro Code and American Specification AISC as detailed in the previous subtitle, where the section is classified as a non-slender section when D/t up to equal 46 or 18 for high-strength steel (S460) or very high-strength steel (S1100) respectively.

Figure 12 shows that the vertical strain of specimens from high-strength steel (S460) ranged from 5.93% to 0.6 % for D/t = 10 to D/t = 100 respectively while it is equal 3.96% and 0.75% for D/t = 10 and 30 respectively for specimens from very high-strength steel (S1100). i.e. when D/t increases the ductility decreases.

For specimens tubes with D/t ≥ 110 for high-strength steel (S460) and D/t ≥ 40 for very high-strength steel (S1100) respectively, it is found that the out-ward deformations were like an elephant's foot buckle that occurred at the two ends as the previous specimens but with little shape. In addition, there are sharp deformations occurred along the length of each tube that was typical to the failure mode of slender tubes due to local buckling behavior as shown in Figures 9 and 10 respectively. All these types of specimens in this range of D/t were not able to reach their yield stress as shown in Figures 11 and 12 because they failed due to local buckling in the elastic stage. It is concluded that these specimens behave as slender tubes.

Figure 9. stress through tube length and failure mode of D/t=10, 50, 60, 100, 110, and D/t=250 (LC1, S460).

Preprints (www.preprints.org) | NOT PEER-REVIEWED | Posted: 13 May 2022 doi:10.20944/preprints202205.0177.v1

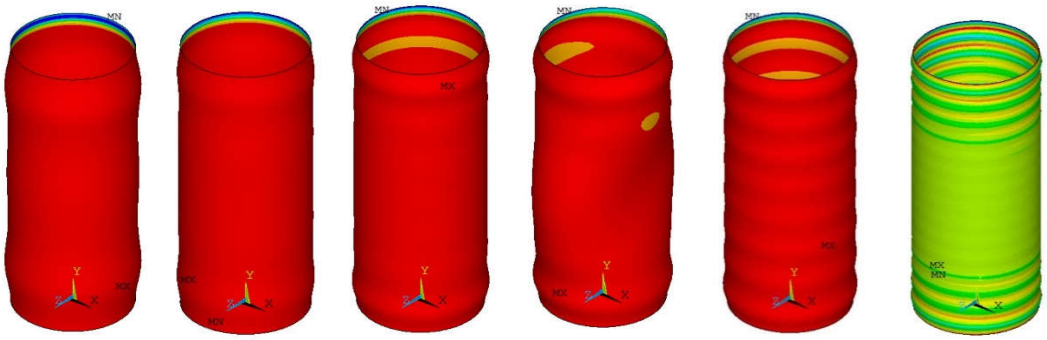

Figure 10. stress through tube length and failure mode of D/t=10, 20, 30, 40, 50 and D/t=250 (LC1, S1100).

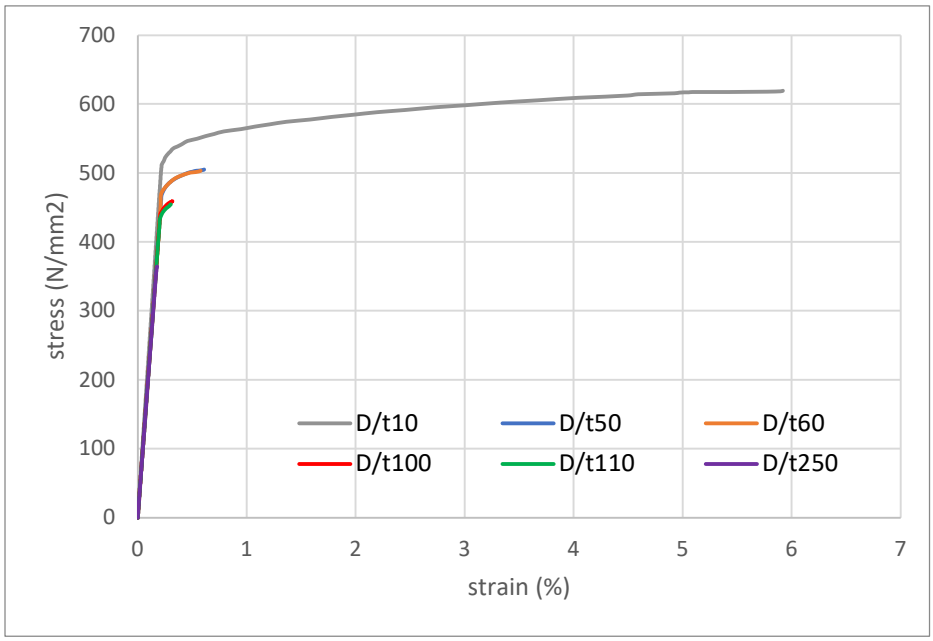

Figure 11. stress strain curve of specimens of D/t=10, 50, 60, 100, 110, and D/t=250 (LC1, S460).

Preprints (www.preprints.org) | NOT PEER-REVIEWED | Posted: 13 May 2022 doi:10.20944/preprints202205.0177.v1

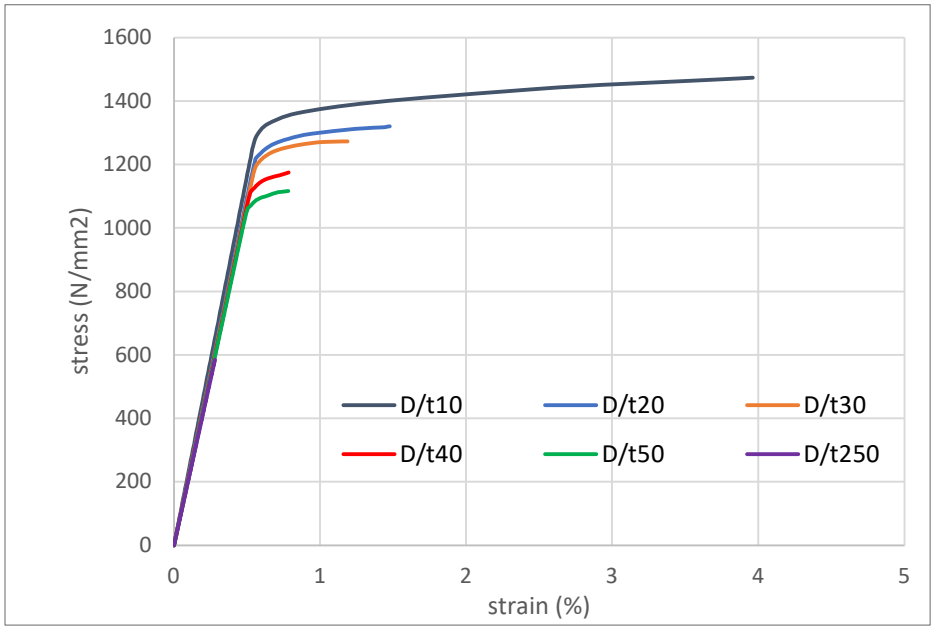

Figure 12. stress-strain curve of specimens of D/t=10, 20, 30, 40, 50, and D/t=250 (LC1, S1100).

4.2. Evaluation of current slenderness limit and design methods

In this section, the results of experimental tests on 105 CHS stub columns by others in previous research were collected to cover a widening range of overall cross-section slenderness besides the studied finite element models. Table 6 shows the range of yield stress or 0.2% proof stress (f_y) obtained from coupon tests, the overall cross-section slenderness (λs), and the number of tests. It is observed that the value of the overall cross-section slenderness (λs) ranged between 37 to 286 ($37 \leq \lambda s \leq 286$) for CHS, a wide range of steel grades with f_y ranged from 357 to 1405 MPa were collated, and the majority of CHS stub columns as shown in Table 6 are made from high-strength steel with f_y higher than 450 MPa. It is noted that the experimental tests on CHS stub columns using high-strength steel remain limited.

Table 6. Others carried out statistics of different experimental tests on *CHS* stub columns.

References	f_y	λs	No, of tests
Junbo Chen [30].	474-970	69-250	16
Ma et al. [34].	1014–1180	101-168	9
Ren et al. [35].	389	94	2
Sakino et al. [36].	283–835	61-195	9
Elchalakani et al. [37]	357–454	37–96	8
Jiao and Zhao [38].	433–1398	44–274	10
Zhao [39].	1341–1405	93–147	12
Wei et al. [40].	216–524	69–286	39
Total			105

Because one of the most important and clear differences in whether the *CHS* column is classified as slender or not is whether the collapse occurred before or after the yield, therefore many of the previous researchers used the ratio (N/N_y), where (N) represents the maximum axial compression load capacity. At the same time, $(N_y = A*f_y)$ denotes the cross-section yield load, which is dependent on the cross-section area (A)and yield stress (f_y).

When the value of $(N/N_y) \geq 1$, it indicates the zone of Class 1–3 requirements for non-slender sections where the failure of a column doesn't occur due to local buckling, while if the value of $(N/N_y) < 1$. It indicates a Class 4 for a slender section where local buckling prevents the yield load from being reached.

Preprints (www.preprints.org) | NOT PEER-REVIEWED | Posted: 13 May 2022 doi:10.20944/preprints202205.0177.v1

Because the classification of the slenderness of section according to Euro Code; EC3, and American Specification; AISC360-16 is dependent on section slenderness (λ_s) and buckling parameter (α), respectively; therefore, the relation between (N/N_y) ratios and section slenderness (λ_s), and buckling parameter (α) are plotted as shown in Figures (13) and (14) respectively for *S460* and Figures (15) and (16) respectively for *S1100* by using results of previous experimental tests and results of FE models by authors. The curve fitting technique is used to require the mathematical equation of relations.

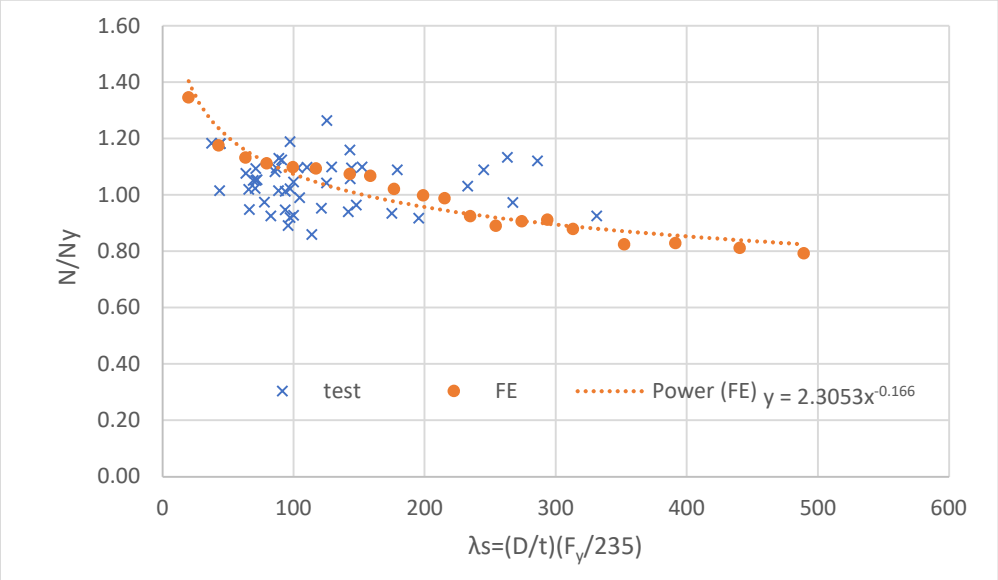

Figure 13. The relation between normalized axial compression and section slenderness of experimental results by others and FE by authors for (S460).

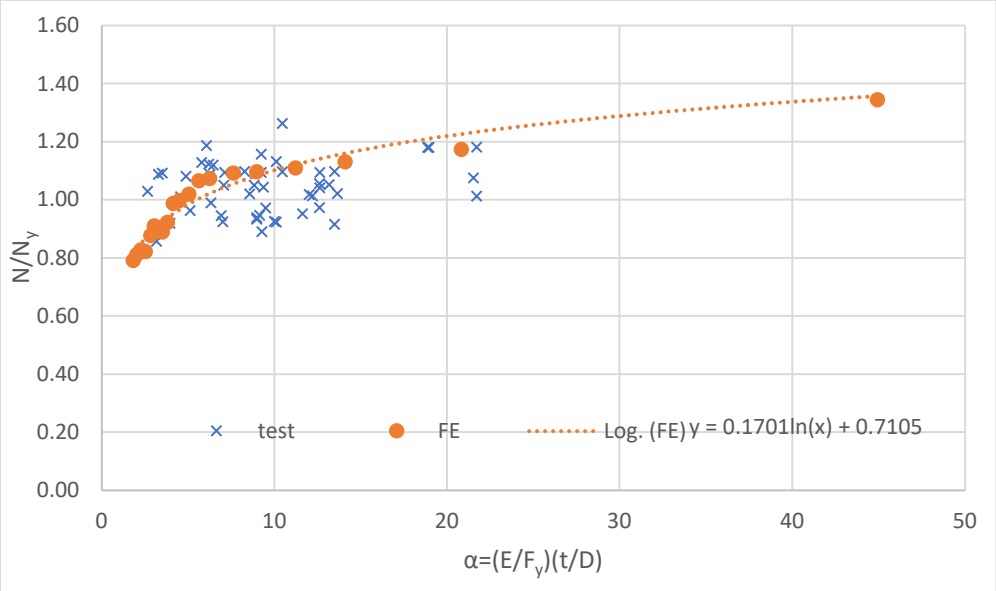

Figure 14. The relation between normalized axial compression and non-dimensional buckling parameter (α) of experimental results by others and FE by authors for (S460).

Preprints (www.preprints.org) | NOT PEER-REVIEWED | Posted: 13 May 2022 doi:10.20944/preprints202205.0177.v1

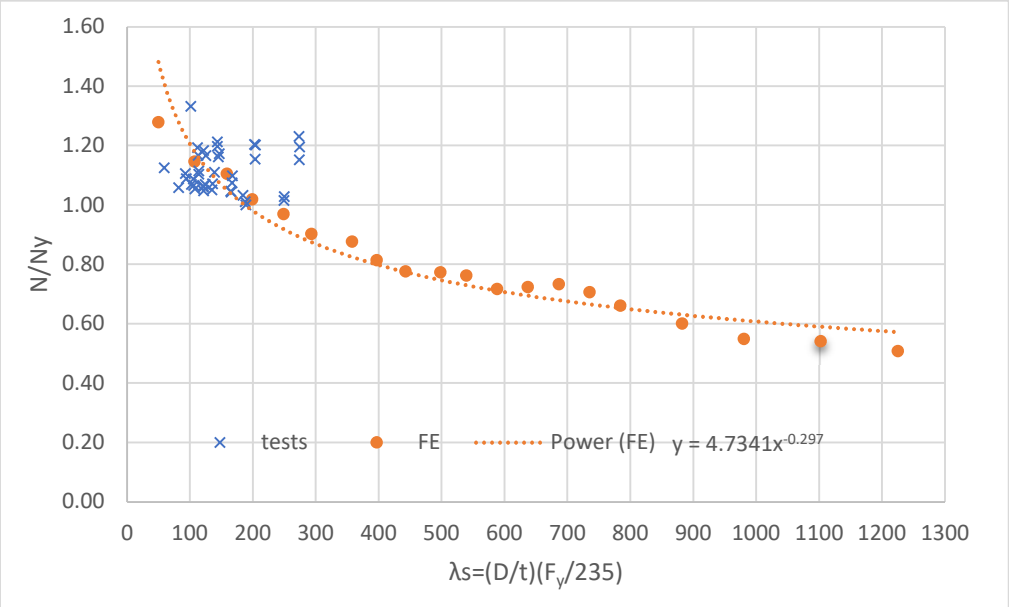

Figure 15. The relation between normalized axial compression and section slenderness of experimental results by others and FE by authors for (S1100).

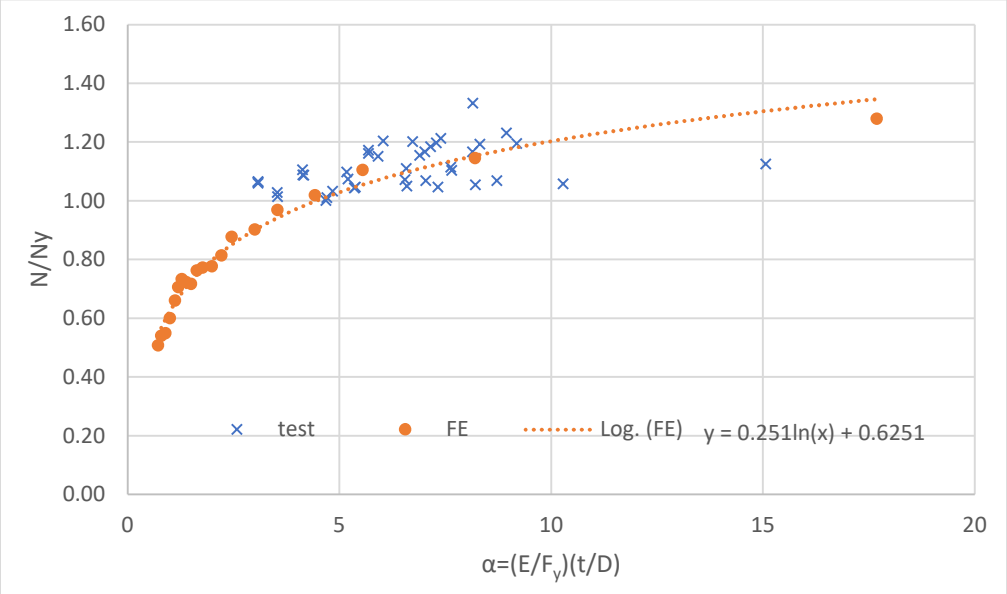

Figure 16. The relation between normalized axial compression and non-dimensional buckling parameter (α) of S1100 of experimental results by others and FE by the authors for (S1100).

Figure 13 shows that all High-strength steel *(S460)* specimens that were studied numerically by authors or almost specimens tested experimentally by others can be classified as non-slender sections because they have normalized axial compression (N/Ny)≥1 despite the values of section slenderness (λs) up to equal 150, while few of specimens tested experimentally support the limits of specifications EC3 or AISC360-16 which equal 90 and 98.3 respectively. Wherefore, it needs an accurate experimental study to determine the accurate limits.

Figure 14 shows that the values of section slenderness (λs) up to equal 180 for all Very high-strength steel *(S1100)* specimens that were studied numerically by authors or experimentally by others; this indicates that the use of EC3 or AISC360-16 limits for high strength steel to check the slenderness of very high strength steel gives conservative results. Therefore, there is a need to derive new modified limits for the section slenderness to suit steel with high and very high strength.

Preprints (www.preprints.org) | NOT PEER-REVIEWED | Posted: 13 May 2022 doi:10.20944/preprints202205.0177.v1

Figures 14 and 16 show the relation between normalized axial compression (N/N_y) and non-dimensional buckling parameter (α) for (S460) and (S1100), respectively, according to the results of previous experimental tests and FE models by the authors. As illustrated in Figures (14) and (16), curve fitting is utilized to obtain the equation for the relationship between normalized axial compression (N/Ny) and buckling parameter (α) for (S460) and (S1100). These equations indicate that the normalized axial compression $(N/N_y) < 1$ when buckling parameters $(\alpha < 4.5)$ *and* $(\alpha < 5.5)$ for (S460) and (S1100), respectively.

Figures 17 and 18 show the relation between normalized axial compression (N/N_y) and section slenderness (λ_s) for (S460) and (S1100), respectively inferred from the results of previous experimental tests, FE models by authors, and finally, the results of design equations according to Euro Code; EC3 and American Specification; AISC360-16. It is shown that the FE models have average results compared to the results of experimental tests. Many boundary parameters affect the accuracy of experimental tests but do not affect the FE models. This gives evidence of the accuracy of the results of the FE models in this study. The technique of curve fitting is used to require the equation of the relation between normalized axial compression (N/N_y) and section slenderness (λ_s) for (S460) and (S1100), as shown in Figures (17) and (18) respectively. These equations indicate that the normalized axial compression $(N/N_y) < 1$ when the section slenderness $(\lambda_s > 150)$ *and* $(\lambda_s > 180)$ for (S460) and (S1100) respectively. This conclusion is confirmed by the results of almost experimental tests for (S460) as shown in Figure 17 and all experimental tests for (S1100) as shown in Figure 18, while the limit of the slenderness of *Euro code 3* of 90 and *AISC-360-the 16* of 98.3. Therefore, the Euro code 3 and AISC-360-16 limits need to be modified by more accurate experimental and numerical studies to determine new limits suitable for high-strength and high-strength steel behavior.

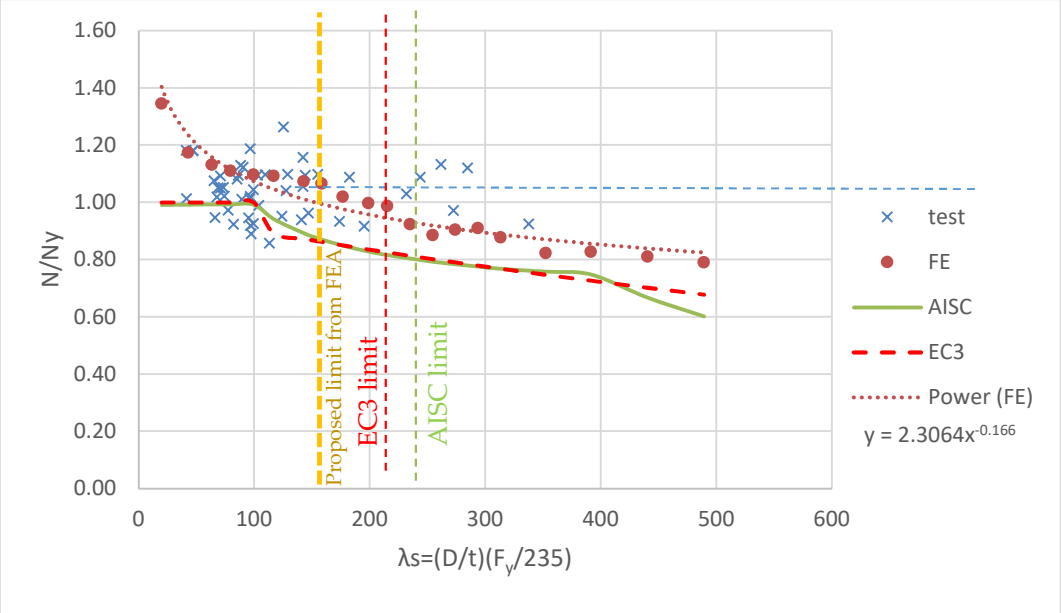

Figure 17. Comparison of normalized static axial load versus section slenderness between experimental results by others, FE by authors and the predicted values of *AISC* and *EC3* standards for (*S460*).

Preprints (www.preprints.org) | NOT PEER-REVIEWED | Posted: 13 May 2022 doi:10.20944/preprints202205.0177.v1

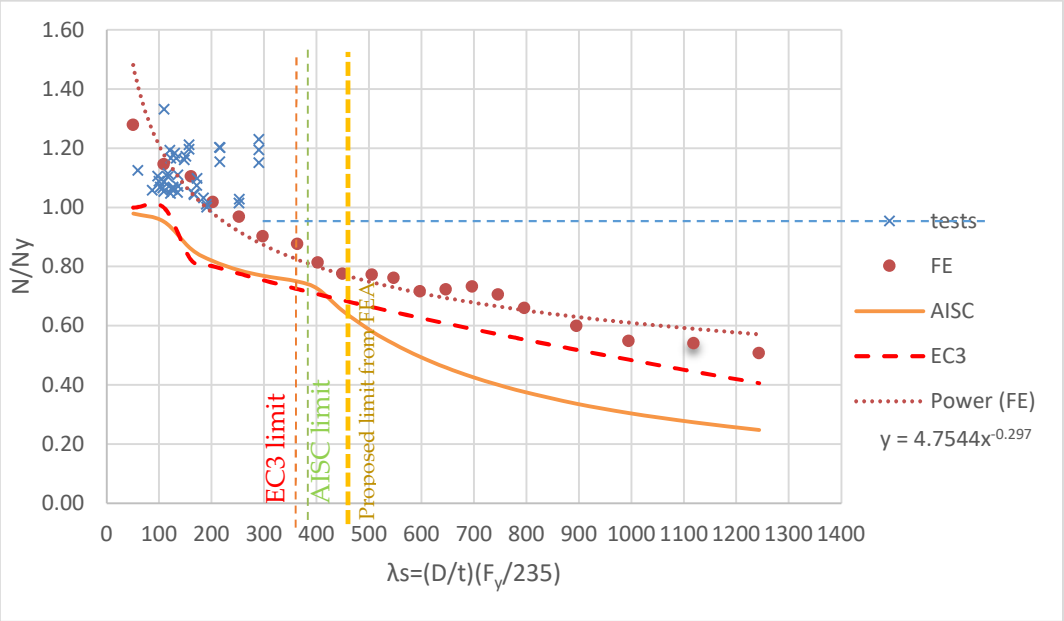

Figure 18. Comparison of normalized static axial load versus section slenderness between experimental results by others, FE by authors, and the predicted values of *AISC* and *EC3* standards for (*S1100*).

The British Standards Institution, BS 5950-1 [3], gave an interaction equation (6) to check the efficiency of high-strength steel cross-sections. It is used here as a base to determine a new simple design method for the design of high and very high strength steel slender circular hollow sections with substituting with the effective cross-section area, which can be calculated as detailed in equations (7) and (8) as follows:

$$\frac{N_{Ed}}{N_{\text{eff,Rd}}} + \frac{M_{y,Ed}}{M_{eff,y,Rd}} + \frac{M_{z,Ed}}{M_{eff,z,Rd}} \leq 1.0 \quad (6)$$

Where:

$M_{eff,y,Rd} = W_{eff,y} * f_y$

$M_{eff,z,Rd} = W_{eff,z} *, f_y$

$N_{eff,Rd} = A_{eff} * f_y$

$N_{c,Rd} = A * f_y$

$M_{y,Ed}$ and $M_{z,Ed}$: are the design bending moments about the major (y-y) and minor (z-z) axes, respectively.

$M_{eff,y,Rd}$ and $M_{eff,z,Rd}$: are the design elastic bending resistance about the major (y-y) and minor (z-z) axes, respectively, based on the effective section properties.

N_{Ed}: is the axial design force

$N_{c,Rd}$ and $N_{eff,Rd}$: are the design cross-section resistances under uniform compression based on the gross and effective section areas, respectively.

$W_{eff,y,}$ and $W_{eff,z}$: are the elastic first moment of inertia about the major (y-y) and minor (z-z) axes, respectively, based on the effective section properties.

A_{eff} : is the effective cross-section area

Based on the modification of the corresponding expressions for CHS given in BS 5950-1 [3], new equations (7) and (8) have been developed to determine the effective cross-section area of CHS for high-strength steel (S460) and ultra-high-strength steel (S1100) respectively. Therefore, the use of interaction equation (6) with using the calculated effective cross-section area from equation (7) or (8) according to the type of steel represents a newly proposed design method.

$$A_{eff} = A \times \left[\frac{90}{D/t} * \frac{235}{fy}\right]^{0.2} \quad (7)$$

Preprints (www.preprints.org) | NOT PEER-REVIEWED | Posted: 13 May 2022 doi:10.20944/preprints202205.0177.v1

$$A_{eff} = A \times [\frac{180}{D/t} * \frac{235}{fy}]^{0.4} \quad (8)$$

Figures (19) and (20) show the comparison between the results of the maximum axial normal force (N) carried by *CHS* normalized by yield load (N_y) was calculated by using the proposed design method and the corresponding results determined from previous experimental tests, finite element models, and the predicted values according to the rules of *AISC-360-16* and *EC3* against the cross-section slenderness parameter for high strength steel (S460) and very high-strength steel (S1100) respectively.

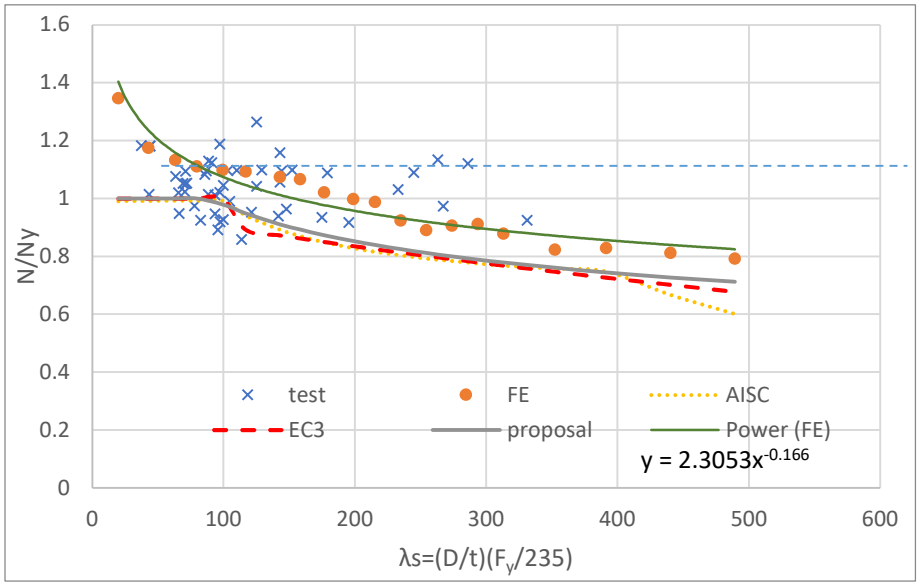

Figure 19. Comparison of normalized static axial load versus section slenderness between the proposed design equation, experimental results by others, FE by authors, and the predicted values of AISC and EC3 standards for high-strength steel (S460).

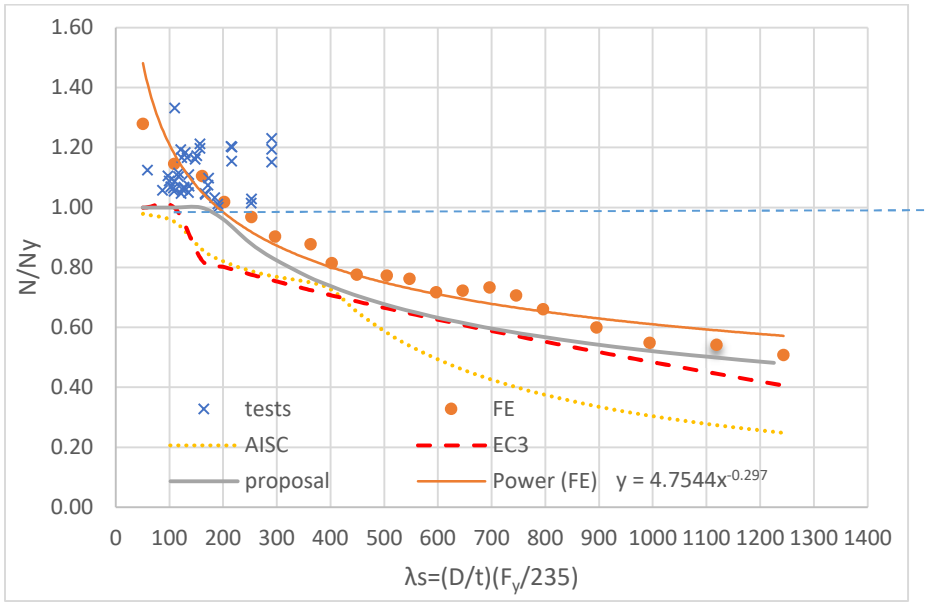

Figure 20. Comparison of normalized static axial load versus section slenderness between the proposed design equation, experimental results by others, FE by authors, and the predicted values of AISC and EC3 standards for high-strength steel (S1100).

It is observed that the results determined by using the rules of *AISC-360-16* and *EC3* standards are more conservative than that calculated by using the proposed method with small values for (S460). At the same time, it is higher for (S1100), especially about [$\lambda s = 180$].

Preprints (www.preprints.org) | NOT PEER-REVIEWED | Posted: 13 May 2022 doi:10.20944/preprints202205.0177.v1

Because the *AISC-360-16* specification for high-strength steel didn't give any information about the design of sections with [$\lambda s > 400$] therefore, the use of its design rules for sections with [$\lambda s < 400$] in this case gives very conservative results than that calculated by using the proposed method and EC3, especially for (S1100).

It's clear that the results of the newly proposed method are more consistent with those determined experimentally and numerically than the predicted values according to the rules of *AISC-360-16* and *EC3* standards for high-strength steel (S460) and very high-strength steel (S1100). Furthermore, it is more accurate and simpler in calculations than the rules of *AISC* and *EC3*.

A summary of the comparison between the ratio between the value of the maximum capacity axial compression load for different studied specimens which were determined from the FE models and those calculated by using the design rules of EN-1993-1-6, AISC-3600-16, and the proposed design method is reported in Tables 7 and 8 for high-strength steel (*S460*) and very high-strength steel (S1100) respectively.

Table 7. Comparison of proposed design method and code predictions with FE results of LC1-460.

No. of specimens:20	N_{FE}/N_{EC3}	N_{FE}/N_{AISC}	$N_{FE}/N_{proposed}$
Mean	1.17	1.17	1.14
COV	0.03	0.05	0.03

Table 8. Comparison of proposed design method and code predictions with FE results of LC1-1100.

No. of specimens:20	N_{FE}/N_{EC3}	N_{FE}/N_{AISC}	$N_{FE}/N_{proposed}$
Mean	1.19	1.53	1.12
COV	0.03	0.19	0.04

The results of the proposed design method are more accurate than those calculated according to *AISC-360-16* and *Euro code 3*.

5. Conclusions

From an analytical study on the limits of the slenderness of high and very high-strength steel circular hollow sections, it can be concluded the following:

1. The limits of the slenderness of High-strength steel circular hollow sections according to AISC-360-16 and EC3 are conservative, concluded from the numerical study and most of the results of previous experimental tests. However, at the same time, few of them support the limits of specifications. Wherefore, it needs an accurate experimental study to determine the accurate limits.
2. There isn't any information about the slenderness limits and design method of Very High-strength steel circular hollow sections given in AISC-360-16 and EC3.
3. The proposed limits of the slenderness for Very High-strength steel circular hollow sections according to this numerical study is [$\lambda s=(D/t)(F_y/235)= 180$], which is in agreement with all results of the previous experimental tests.
4. New simple design equations were developed for slender circular hollow sections from high and ultra-high-strength steel.
5. The results of the newly proposed method are more consistent with those determined experimentally and numerically than the predicted values according to the rules of *AISC-360-16* and *EC3* standards for high-strength steel and very high-strength steel. Furthermore, it is more accurate and simpler in calculations than the rules of *AISC* and *EC3*.
6. The *AISC-360-16* specification for high-strength steel didn't give any information about the design of slender sections with [$\lambda s > 400$] while it is covered in the proposed method and also EC3.

 doi:10.20944/preprints202205.0177.v1

7. The design of circular hollow sections by using the rules of *AISC-360-16* and *EC3* standards is more conservative than that by using the proposed method with small values for (S460) while it is higher for (S1100), especially about [$\lambda s = 180$].

6. Patents

Not applicable.

Supplementary Materials: Not applicable.

Author Contributions: Equal share authors.

Funding: Not applicable.

Data Availability Statement: Not applicable.

Acknowledgments: Not applicable.

Conflicts of Interest: Not applicable.

References

1. D. Dutta, Structures with Hollow Sections, Wiley VCH, Weinheim, 2002.
2. European Committee for Standardization (CEN), EN 1993-1-1:2005 Euro code 3: Design of Steel Structures — Part 1-1: General Rules and Rules for Buildings, 2005.
3. British Standards Institution, BS 5950-1:2000 Structural Use of Steelwork in Building — Part 1: Code of Practice for Design — Rolled and Welded Sections, 2000.
4. European Committee for Standardization (CEN), EN 1993-1-6:2007 Euro code 3: Design of Steel Structures — Part 1-6: Strength and Stability of Shell Structures, 2007.
5. European Committee for Standardization (CEN), EN 1999-1-1:2007 Euro code 9: Design of Aluminum Structures — Part 1-1: General Structural Rules, 2007.
6. American Institute of Steel Construction, ANSI/AISC 360-16 Specification for Structural Steel Buildings, 2016.
7. Standards Australia, AS 4100-1998 Steel Structures, 1998.
8. M. Ashraf, L. Gardner, D.A. Nethercot, Resistance of stainless steel CHS columns based on cross-section deformation capacity, J.Constr. Steel Res. 64 (9) (2008) 962–970.
9. Ren, Qing-Xin, et al. "Experiments on special-shaped CFST stub columns under axial compression." Journal of Constructional Steel Research 98 (2014): 123-133.
10. Ma, Jia-Lin, Tak-Ming Chan, and Ben Young. "Cold-formed high strength steel tubular beam-columns." Engineering Structures 230 (2021): 111618.
11. O'Shea, Martin D., and Russell Q. Bridge. "Local buckling of thin-walled circular steel sections with or without internal restraint." Journal of Constructional Steel Research 41.2-3 (1997): 137-157.
12. CHUNG, Jinan. "High-strength concrete-filled square tube columns subjected to axial loading." The Seventh East Asia-Pacific Conference on Structural Engineering & Construction. Vol. 2. 1999.
13. Guo, Lanhui, et al. "Behavior of thin-walled circular hollow section stub columns under axial compression." International Journal of Steel Structures 16.3 (2016): 777-787.
14. Wang, Hui, et al. "Experimental and numerical study on the stability capacity of Q690 high-strength circular steel tubes under axial compression." International Journal of Steel Structures 17.3 (2017): 843-861.
15. Zhao, Xiao-Ling. "Section capacity of very high strength (VHS) circular tubes under compression." Thin-Walled Structures 37.3 (2000): 223-240.
16. Jiao, Hui, and X-L. Zhao. "Imperfection, residual stress and yield slenderness limit of very high strength (VHS) circular steel tubes." Journal of Constructional Steel Research 59.2 (2003): 233-249.
17. Ma, Jia-Lin, Tak-Ming Chan, and Ben Young. "Experimental investigation on stub-column behavior of cold-formed high-strength steel tubular sections." Journal of Structural Engineering 142.5 (2016): 04015174.
18. CEN (EUROPEAN COMMITTEE FOR STANDARDISATION). BS EN-1993-1-3 Eurocode 3—design of steel structures—Part 1-3: general rules—supplementary rules for cold-formed members and sheeting. London: British Standards Institution; 2006.
19. Gardner, L., and D. A. Nethercot. 2004b. "Numerical modelling of stainless-steel structural components—A consistent approach." J. Struct.Eng. 130 (10): 1586–1601.
20. Elchalakani M, Zhao XL, Grzebieta R. Tests on concrete filled double-skin (CHS outer and SHS inner) composite short columns under axial compression. Thin Walled Struct. 2002;40(5):415–41.
21. CEN (EUROPEAN COMMITTEE FOR STANDARDISATION). BS EN-1993-1-12 Eurocode3: design of steel structures—Part 1-12: additional rules for the extension of EN 1993 up to steel grades S 700. London: British Standards Institution; 2007.

 doi:10.20944/preprints202205.0177.v1

22. CEN (EUROPEAN COMMITTEE FOR STANDARDISATION). BS EN10219-1 Cold formed welded structural hollow sections of non-alloy and fine grain steels. Part 1—technical delivery requirements. London: British Standards Institution; 2006.
23. A514/A514M - 18e1, Standard specification for high-yield-strength, quenched and tempered alloy steel plate, suitable for welding, American Society for Testing and Materials (ASTM), West Conshohocken, 2018.
24. A1085/A1085M - 15, Standard Specification for Cold-Formed Welded Carbon Steel Hollow Structural Sections (HSS), American Society for Testing and Materials (ASTM), West Conshohocken, 2015.
25. AISI S100. North American specification for the design of cold-formed steel structural members. Washington: American Iron and Steel Institute (AISI); 2016.
26. Meng, Xin, and Leroy Gardner. "Cross-sectional behaviour of cold-formed high strength steel circular hollow sections." Thin-Walled Structures 156 (2020): 106822.
27. by Gabriel J. DeSalvo and John A. Swanson. ANSYS Engineering Analysis System User's Manual. Houston, Pa.: Swanson Analysis Systems, 1985.
28. Banerjee, Biswajit, et al. "Comparison of ANSYS elements SHELL181 and SOLSH190." (2011).
29. Ma JL, Chan TM, Young B. Material properties and residual stresses of cold-formed high strength steel hollow sections. J Construct Steel Res 2015; 109:152–65.
30. Chen, Junbo, Tak-Ming Chan, and Amit H. Varma. "Stub Column Behavior of Cold-Formed High-Strength Steel Circular Hollow Sections under Compression." Journal of Structural Engineering 146, no. 12 (2020): 04020277.
31. X. Meng, L. Gardner, Simulation and design of semi-compact elliptical hollow sections, Eng. Struct. 202 (2020) 109807.
32. Gardner, L., and D. A. Nethercot. 2004b. “Numerical modeling of stainless-steel structural components—A consistent approach.” J. Struct.Eng. 130 (10): 1586–1601.
33. Guo, Lanhui, et al. "Behavior of thin-walled circular hollow section stub columns under axial compression." International Journal of Steel Structures 16.3 (2016): 777-787.
34. Ma JL, Chan TM, Young B. Experimental investigation on stub-column behavior of cold-formed high-strength steel tubular sections. J Struct Eng 2016;142(5):04015174.
35. Ren, Qing-Xin, et al. "Experiments on special-shaped CFST stub columns under axial compression." Journal of Constructional Steel Research 98 (2014): 123-133.
36. Sakino K, Nakahara H, Morino S, Nishiyama I. Behavior of centrally loaded concrete-filled steel-tube short columns. J Struct Eng 2004;130(2):180–8.
37. Elchalakani M, Zhao XL, Grzebieta R. Tests on concrete filled double-skin (CHS outer and SHS inner) composite short columns under axial compression. Thin-Walled Struct 2002;40(5):415–41.
38. Jiao, Hui, and X-L. Zhao. "Imperfection, residual stress and yield slenderness limit of very high strength (VHS) circular steel tubes." Journal of Constructional Steel Research 59.2 (2003): 233-249.
39. Zhao XL. Section capacity of very high strength (VHS) circular tubes under compression. Thin-Walled Struct 2000; 37:223–40.
40. Wei S, Mau ST, Vipulanandan C, Mantrala SK. Performance of new sandwich tube under axial loading: experiment. J Struct Eng 1995;121(12):1806–14.